

## Charge transfer and memory loss in keV oxygen-ion scattering from Cu(001)

A. C. Lavery, C. E. Sosolik, C. A. Keller, and B. H. Cooper\*

*Laboratory of Atomic and Solid State Physics, Cornell University, Ithaca, New York 14853-2501*

(Received 25 May 1999)

Oxygen ion and neutral atom yields were measured for  $O^+$  and  $O^-$  ions incident on a clean Cu(001) surface for ion energies from 0.4 to 5 keV. Scattering geometries were chosen that simplify the selection of single collisions between the incident ions and surface atoms and consequently also simplify the identification of the charge transfer mechanisms occurring in the O-Cu system. It was found that the ratio of  $O^+$  to  $O^-$  ions is independent of the incident ion charge state, demonstrating that memory loss occurs over the entire range of energies and scattering geometries investigated. From general arguments based on the energies of the electronic states of the O-Cu system, we attribute the formation of scattered  $O^-$  ions and neutral O atoms to a resonant charge transfer process. Evidence is presented that the formation of  $O^+$  ions is due to a hard collision between the incident ions and top layer surface atoms. Similar measurements were made for low energy ( $\leq 4$  keV)  $C^+$  ions incident on Cu(001), over the same range of scattering geometries. The behavior of the single scattering peaks in the  $C^-$  spectra is also consistent with a resonant charge transfer process. No  $C^+$  ions were observed in the scattered flux for all energies and scattering geometries investigated.

### I. INTRODUCTION

When low energy ions are scattered from metallic surfaces it is found that there are particles in the scattered flux with charge states that differ from that of the incident ions. There are many different mechanisms, such as resonant and Auger charge transfer, by which electrons may be exchanged between the incident ions and the surface. It is these processes that are responsible for the change in the incident ion charge state. Ion-surface scattering experiments allow the dynamics of charge transfer to be probed in a controlled manner. In particular, the nonadiabaticity of the charge transfer can be investigated by varying the velocity of the scattered particles through adjustments of the incident ion's energy and scattering geometry. Understanding dynamical charge transfer is critical for understanding many processes that involve atoms interacting with surfaces, such as chemisorption and molecular dissociation. Charge transfer is also central to surface analysis techniques such as secondary ion mass spectroscopy (SIMS).

In the present work we use low energy ion scattering to study the charge transfer that occurs when incident  $O^+$  and  $O^-$  ions are scattered from a clean, single-crystal Cu(001) surface. As has been discussed in our previous work,<sup>1</sup> there are many effects that need to be included in the analysis of such a complex system. One of the most interesting aspects is the presence of multiple equivalent atomic  $p$  electrons on the oxygen that can participate in the charge exchange. This is in contrast to the better understood alkali ion-surface scattering systems where at most one  $p$  electron in the outer atomic orbital is involved. There have been several recent theoretical<sup>2-6</sup> and experimental<sup>7-9</sup> studies aimed at better understanding the role of multiple equivalent  $p$  electrons in charge transfer processes in systems similar to that under investigation here.

The goals of this paper are multifold. First we present results of a thorough investigation of memory loss for the O-Cu system. Throughout this paper we will consider that

memory loss has occurred if the measured scattered ion yields are independent of the charge state of the incident ions. Our previous work involving the scattering of incident  $O^+$  from Cu(001) has shown that there is a considerable fraction of  $O^+$  ions in the scattered flux.<sup>1</sup> This was a surprising observation if one considers a simple picture of resonant charge transfer. One possible explanation for the observed  $O^+$  ion yields was that memory of the incident ion charge state was not completely lost during the interaction of the ion with the surface. Here we show that this is not the case and demonstrate that memory loss is complete over the entire range of incident energies and scattering geometries under investigation. From this observation we draw some conclusions about the mechanisms that lead to memory loss. There have been other investigations of memory loss,<sup>8,10</sup> but it has never before been tested for ions with such high incident and scattered velocities perpendicular to the surface.

The second goal was to obtain a quantitative measurement of final charge state yields over an extensive range of incident ion energies and scattering geometries. Recently, much work has gone into developing multistate models of resonant charge transfer.<sup>3,11,12</sup> One many-body model that describes the key elements of resonant charge transfer in multistate systems has been developed by Marston *et al.*<sup>11</sup> and used to successfully reproduce measurements for alkali ion-surface scattering.<sup>13,14</sup> The next step is to develop the ability to model resonant charge transfer in more complex systems, such as O-Cu. This system is more complex, not only because multiple oxygen  $p$  electrons are involved in the resonant charge transfer, but because it may also be necessary to incorporate additional charge transfer mechanisms. For instance, to explain the observed positive ion yields it may be necessary to include effects due to the hard collision between the incident ions and surface atoms. The data we have obtained here will be useful for comparison with the results of future charge transfer models which correctly incorporate the relevant multistate aspects of the O-Cu system.

Finally, we present the results obtained from the scatter-

ing of low energy  $C^+$  ions from a clean Cu(001) surface, measured over the same range of incident and final scattering geometries. Neutral C has two electrons in the  $2p$  shell, instead of two holes as in neutral O, making this an interesting complementary system to study.

The organization of this paper is as follows. In Sec. II, we present the experimental apparatus and measurement and analysis techniques. In Sec. III, we present the experimental scattering results for 1–5 keV  $O^-$  ions incident on Cu(001) at  $45^\circ$ . Section III A compares the scattered  $O^+/O^-$  ratios obtained for both incident  $O^+$  and  $O^-$  ions, which demonstrate that memory loss of the incident charge occurs. In Sec. III B we present a complete set of measurements of the scattered  $O^+/O^-$  ratios over a wide range of final scattering angles. Section III C presents the absolute ion and neutral atom yields. These data are necessary for comparison to the results of multistate models of charge transfer. We also present the results of scattering low energy ( $\leq 4$  keV)  $C^+$  from Cu(001), in Sec. III D. A brief qualitative description of the charge transfer mechanisms relevant to these systems is presented in Sec. IV, together with a discussion of the data as it relates to these mechanisms. We summarize our results in Sec. V.

## II. EXPERIMENTAL TECHNIQUE AND ANALYSIS

These experiments were performed in an ultra high vacuum (UHV) system that has been described in detail elsewhere.<sup>15–17</sup> Only the features relevant to the present work are summarized here.

The UHV chamber used for obtaining the measurements presented in this study was equipped with a beamline for producing well-collimated, monoenergetic, low, and hyperthermal energy ion beams in the energy range from 5 eV to 10 keV.<sup>17</sup> The measurements described in this paper were carried out using  $O^+$  and  $O^-$  ions extracted from a Colutron ion source.<sup>18</sup> A source gas mixture of 15%  $O_2$ –85% Ne was used for the production of the  $O^+$  ions, and pure  $N_2O$  gas was used for the  $O^-$  ions. Pure  $CO_2$  gas was used to produce  $C^+$  beams.

The Cu(001) single crystal was prepared by standard sputter and anneal cycles. Surface cleanliness and long range order were monitored using Auger electron spectroscopy (AES) and low energy electron diffraction (LEED), respectively. The base pressure was  $3 \times 10^{-11}$  Torr and operating pressures were below  $2 \times 10^{-10}$  Torr. Before each measurement the sample was cleaned by annealing for 2 min at  $700^\circ C$ , sputtering for 10 min with a  $2 \mu A$  beam of 500 eV  $Ar^+$ , and then annealing again for 2 min at  $600^\circ C$ .

The beam was incident on the Cu(001) sample along the  $\langle 100 \rangle$  azimuth. LEED was used to align the  $\langle 100 \rangle$  azimuth of the sample to within  $\pm 2^\circ$  of the incident ion beam direction. The azimuthal position was then fine-tuned to  $\pm 0.5^\circ$  by monitoring the scattered ion beam intensity, which is highly sensitive to the azimuthal orientation. Both the incident ( $\theta_i$ ) and final ( $\theta_f$ ) scattering angles were measured from the surface normal (see the inset in Fig. 1).

A time-of-flight (TOF) spectrometer<sup>15</sup> and a hemispherical electrostatic analyzer (ESA), both mounted on a rotatable platform, were used to detect the scattered particles. The ESA entrance optics provided 1.5% energy resolution and an

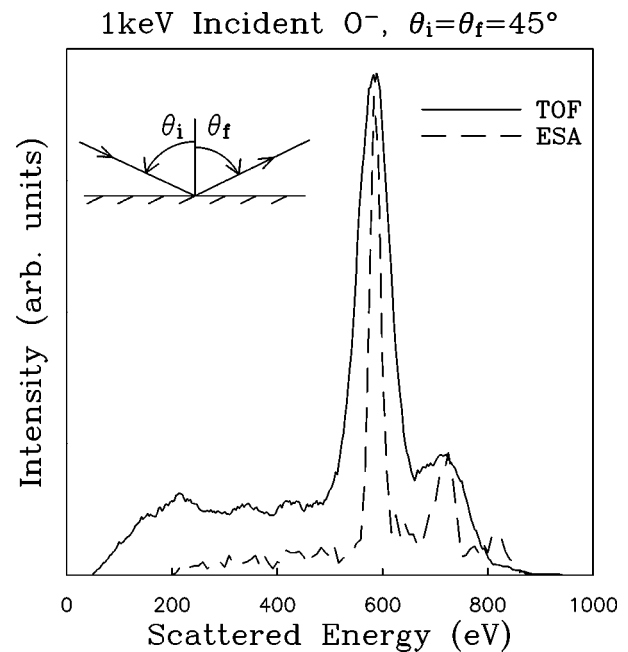


FIG. 1. Typical ESA and TOF spectra for 1 keV  $O^-$  incident on Cu(001)  $\langle 100 \rangle$  with  $\theta_i = \theta_f = 45^\circ$ . The dashed line represents the ESA spectra for scattered  $O^-$ , and the solid line is the TOF spectra for the scattered totals (neutrals and ions). Due to the short path length from the sample to the TOF detector, the resolution for the spectra taken with the ESA detector is better than for spectra taken with the TOF detector. The inset shows the in-plane scattering geometry used throughout this paper, where  $\theta_i$  and  $\theta_f$  are the incident and final scattering angles, respectively, always measured from the surface normal.

angular acceptance of  $\pm 1^\circ$  full width. Channel electron multipliers (CEM)<sup>19</sup> operated in the pulse counting mode and located at the exit of the TOF analyzer and the ESA served as detectors. The CEM at the exit of the ESA has been calibrated for the different efficiencies of detecting positive and negative ions.<sup>20</sup>

The analysis of the present data focuses on quasisingle (QS) trajectory scattering from top layer atoms. QS trajectories involve incident ions that undergo a collision primarily with a single surface atom. Figure 1 shows typical ESA and TOF measurements of the scattered particles for 1 keV  $O^-$  ions incident at  $45^\circ$ . Using our classical trajectory simulation code SAFARI (Ref. 21) with a ZBL potential<sup>22,23</sup> it is possible to identify the most prominent peak in Fig. 1 as the QS peak. This will be discussed in more detail in Sec. III D. Other trajectory types also occur, but we do not focus on these since they result from multiple collisions and complicate the interpretation of the data. The analysis was further simplified by restricting the incident angle to  $45^\circ$ , minimizing the scattering from deeper layers due to blocking by the first layer atoms. Classical trajectory analysis indicates that for ions incident at  $45^\circ$ , the only trajectories that contribute to the QS peaks are those that involve QS collisions with surface layer atoms. For more details on the classical trajectory analysis and interpretation of the spectra see Ref. 1.

For each incident ion energy, charge species, scattering geometry, and method of data acquisition (ESA and TOF), the data analysis consisted of separating the QS peak from the background and calculating the integrated intensity of the

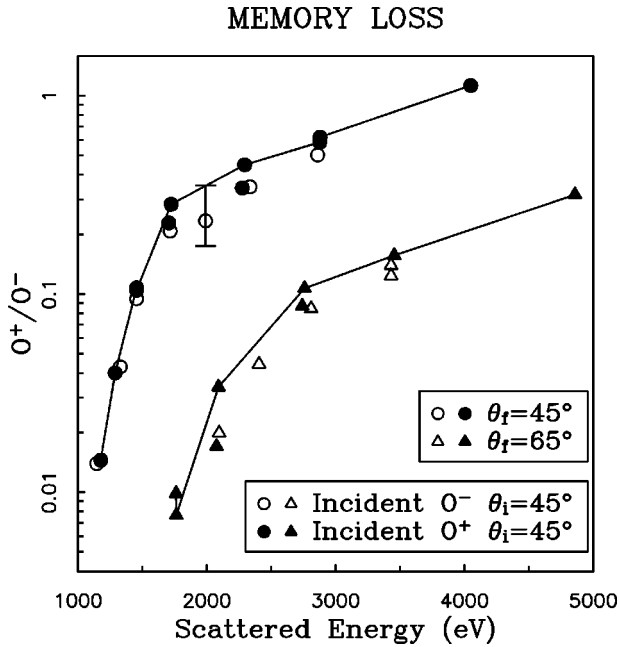


FIG. 2. Evidence for memory loss.  $O^+/O^-$  ratios plotted as a function of the scattered energy, for  $O^+$  and  $O^-$  ions incident on Cu(001)  $\langle 100 \rangle$  with  $\theta_i = 45^\circ$ . These data were taken with the ESA spectrometer. The  $O^+/O^-$  ratios for the incident  $O^+$  ions were also presented in our previous work (Ref. 1). Closed symbols represent incident  $O^+$  ions, open symbols represent incident  $O^-$  ions. The circles correspond to a final scattering angle  $\theta_f = 45^\circ$ , and the triangles correspond to a final scattering angle of  $\theta_f = 65^\circ$ . A typical error bar is shown. The lines are included to *guide the eye* and, for clarity, not all data points were connected.

peak. This was achieved by fitting each spectrum to a Gaussian and linear background, and then integrating the area under the Gaussian. For the ESA spectra it was necessary to correct for the transmission function of the detector and to calibrate for the different CEM efficiencies for detecting positive and negative ions. It was not possible to correct the TOF data for the different efficiencies of the CEM for detecting neutral, positive and negative oxygen, since this calibration was not available. Instead, it was assumed that these efficiencies were equal. At the energies of this experiment we do not expect these corrections to be significant.<sup>20</sup>

The TOF spectrometer permits the measurement of either the total number of scattered particles, which includes both ions and neutral atoms, or of the scattered neutral atoms alone. This measurement is performed by pulsing a rejection voltage on two parallel plates, located at the entrance to the TOF spectrometer, that either allows all scattered particles to pass, or sweeps away positive and negative ions, allowing only the neutral atoms to get through. The analysis of the TOF spectra then determines the fraction of neutral oxygen atoms in the scattered flux  $P^0$ . To complete the analysis it was also necessary to obtain the  $O^+$  to  $O^-$  ratio  $R$  from the ESA energy spectra. It should be noted that both detectors allowed only the determination of the charge state of the scattered particles and did not distinguish between excited and ground state particles. Combining the ESA and TOF measurements, it was then possible to extract the absolute yields  $P^+$  and  $P^-$  of scattered  $O^+$  and  $O^-$ , respectively. These yields are given by the following expressions:

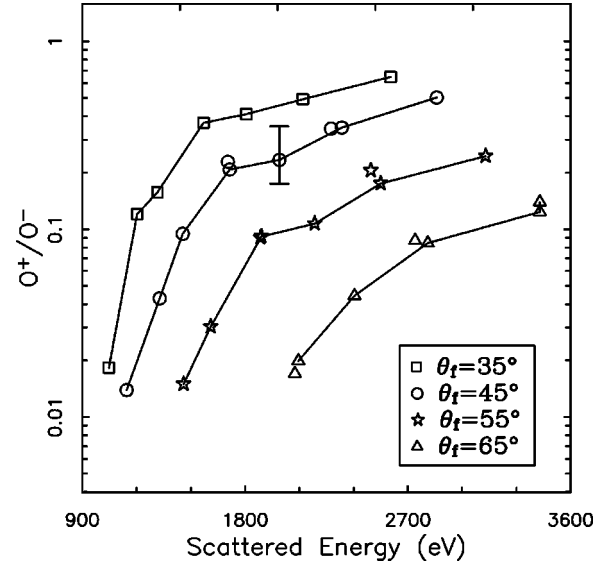


FIG. 3.  $O^+/O^-$  ratio for  $O^-$  ions incident on Cu(001)  $\langle 100 \rangle$ ,  $\theta_i = 45^\circ$ , taken with the ESA spectrometer, and plotted as a function of the scattered energy. The squares correspond to a final scattering angle of  $\theta_f = 35^\circ$ , the circles to  $\theta_f = 45^\circ$ , the stars to  $\theta_f = 55^\circ$ , and the triangles to  $\theta_f = 65^\circ$ . A typical error bar is shown. The lines are included to *guide the eye* and, for clarity, not all data points were connected.

$$P^+ = \left( \frac{R}{1+R} \right) (1 - P^0)$$

and

$$P^- = \left( \frac{1}{1+R} \right) (1 - P^0).$$

### III. RESULTS

#### A. ESA data: Evidence for memory loss

One of the initial goals of this study was to investigate memory loss in the O-Cu system. With that aim in mind, we used the ESA detector to measure the ratio of  $O^+$  to  $O^-$  ions,  $R$ , in the scattered flux, for both positive and negative incident ions. Figure 2 shows the results of this measurement for ions incident at  $45^\circ$  and for  $\theta_f = 45^\circ$  and  $65^\circ$ . The incident energy,  $E_i$ , ranged from 0.4–5 keV for the incident  $O^-$  and from 0.4–7 keV for the incident  $O^+$ . Although data were taken for incident energies below 1.8 keV, the scattered  $O^+$  ion yields were below the limits of detectability. From Fig. 2, it is apparent that the  $O^+/O^-$  ratios are indistinguishable for the two incident charge species, for both values of  $\theta_f$ . This indicates that over the range of incident energies and scattering geometries investigated, memory loss of the incident charge state is complete.

#### B. ESA data: $O^+/O^-$ ratio

A more complete data set showing the  $O^+/O^-$  ratios, for  $O^-$  incident at  $45^\circ$  with various final scattering angles, is presented in Fig. 3. It can be seen that for a given scattered energy, the  $O^+/O^-$  ratio is larger for the more normal scattering geometries. As will be discussed in Sec. IV A, the  $O^-$

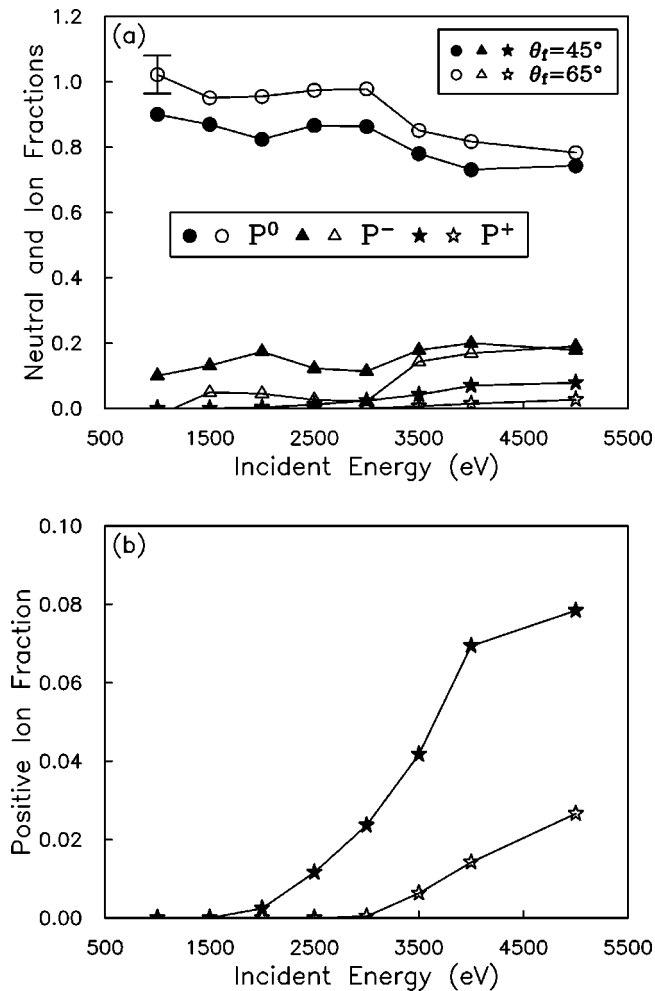


FIG. 4. Absolute yields. (a)  $O^+$ ,  $O^-$ , and neutral oxygen fractions, as a function of the *incident* energy, for  $O^-$  ions incident at  $\theta_i = 45^\circ$ . Circles represent the neutral atom fractions, triangles the negative ion fractions, and the stars the positive ion fractions. The closed symbols correspond to a final scattering angle of  $\theta_f = 45^\circ$ , and the open symbols correspond to  $\theta_f = 65^\circ$ . A typical error bar is shown. (b)  $O^+$  fraction as a function of the incident energy for  $O^-$  incident at  $\theta_i = 45^\circ$ . The closed symbols correspond to a final scattering angle of  $\theta_f = 45^\circ$ , and the open symbols to  $\theta_f = 65^\circ$ .

fraction is expected to increase with decreasing  $\theta_f$  due to resonant charge transfer. However, since the  $O^+/O^-$  ratios increase with decreasing  $\theta_f$ , we conclude from these data that the  $O^+$  fraction must be changing more rapidly than the  $O^-$  fraction. This is supported by the TOF data presented in the next section.

### C. TOF data: Absolute yields

Although many conclusions can be drawn from the  $O^+/O^-$  ratios about the charge transfer processes occurring in the O-Cu system, it is necessary to obtain absolute yields for direct comparison with a theoretical model. The absolute yields of  $O^+$ ,  $O^-$ , and neutral O are shown in Fig. 4(a) as a function of the *incident* energy, for  $\theta_i = 45^\circ$  and for  $\theta_f = 45^\circ$  and  $65^\circ$ . It can be seen that the majority of the scattered flux is neutral. Furthermore, the neutral O fraction is higher for  $\theta_f = 65^\circ$  than for  $\theta_f = 45^\circ$ ; for both angles, the neutral yields decrease slightly as the incident ion energy is

increased. From this figure it can also be seen that the negative ion yield increases gradually with incident ion energy and is larger for  $\theta_f = 45^\circ$ .

Figure 4(b) shows only the  $O^+$  ion fraction  $P^+$  as a function of the incident ion energy. For  $\theta_f = 65^\circ$ ,  $P^+$  turns on at an incident ion energy of 3 keV, whereas at  $\theta_f = 45^\circ$ ,  $P^+$  turns on at a lower incident ion energy, approximately 2 keV. As we will see in Sec. IV D, the behavior of the  $O^+$  yields is consistent with the idea that a hard collision is responsible for producing positive ions.<sup>8,24-29</sup>

### D. Comparison of carbon and oxygen ESA spectra and backgrounds

The ESA spectrometer was also used to take data for low energy ( $\leq 4$  keV)  $C^+$  incident on Cu(001), over a similar range of scattering geometries. Our goal was to investigate the charge transfer processes occurring in a system very similar to the O-Cu system already under investigation. C and O are not only close in mass, relative to Cu, but have similar atomic orbital symmetries.

The data were taken with incident  $C^+$  ions since, in our source,<sup>30</sup> the production of positive ion beams is significantly easier than that of negative ion beams. The most important observation we made was that there were no  $C^+$  ions in the scattered flux for any incident ion energy or scattering geometry under investigation, clearly indicating that there was no survival of incident  $C^+$  ions.

Figure 5 compares angular spectra for scattered  $O^-$ ,  $O^+$ , and  $C^-$  ions. These angular spectra are a compilation of several individual ESA energy spectra taken at different final scattering angles, plotted as a function of the scattered energy. Each spectrum has been normalized by the incident current on the sample, allowing the magnitude of the peaks to be compared directly. Each individual ESA spectrum is made up of a background and a QS peak. Here we are interested in the shape of the envelope that connects the apex of each of the QS peaks that make up an angular spectrum. These are qualitatively different for the scattered  $O^-$  and  $C^-$  angular spectra shown in Fig. 5. The envelope shape observed for the  $O^-$  angular spectrum has been discussed in detail in Ref. 1. It is determined predominantly by the classical scattering cross section, which has a maximum at  $\theta_f = 65^\circ$ .<sup>31</sup> The  $C^-$  envelope, on the other hand, reaches a maximum at the most normal scattering geometries, at  $\theta_f = 15^\circ$ , which is where the  $C^-$  ion spends the least amount of time close to the surface on the outward trajectory. In fact, the shape of the  $C^-$  angular spectrum more closely resembles that of the  $O^+$  angular spectrum shown in Fig. 5(b). As will be discussed later, the observed  $C^-$  trends are consistent with a dynamical model of resonant charge transfer.

Information about the charge transfer processes occurring in these systems can also be obtained from a closer inspection of the magnitudes of the backgrounds in the ESA spectra. The magnitude of the background depends on the incident ion species, the scattering geometry, the incident ion energy, and the final charge state. As is discussed in detail in Ref. 1, the backgrounds for the scattered  $O^-$  spectra are typically larger than those for the  $O^+$  spectra. This is illustrated in Fig. 6(a) for 4 keV  $O^-$  incident at  $\theta_i = 45^\circ$ . This can also be seen by comparing Figs. 5(a) and 5(b). Figure 6(b)

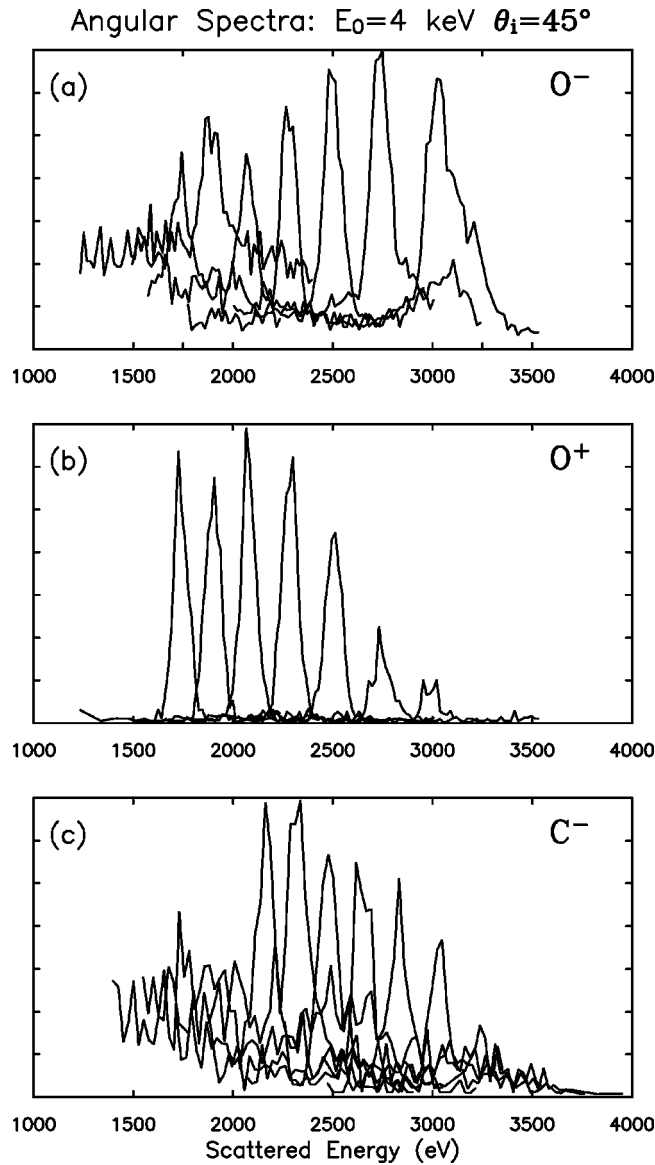


FIG. 5. Comparison of ESA angular spectra for (a) incident  $O^-$  and scattered  $O^-$ , (b) incident  $O^-$  and scattered  $O^+$ , and (c) incident  $C^+$  and scattered  $C^-$ . The incident energy was 4 keV and  $\theta_i = 45^\circ$ . Each angular spectrum is made up of several individual ESA energy spectra, in which the most prominent feature is the QS peak. The final angles included in the spectra are, from left to right,  $\theta_f = 15^\circ, 25^\circ, 35^\circ, 45^\circ, 55^\circ, 65^\circ, 75^\circ$ . For details on how to construct these angular spectra see Sec. III D. There was no observable scattered  $C^+$  signal.

shows a scattered spectrum for 4 keV  $C^+$  incident at  $\theta_i = 45^\circ$ . A comparison of Figs. 6(a) and 6(b) shows that the scattered  $C^-$  and  $O^-$  spectra have very similar backgrounds.

To gain a detailed understanding of the origin of the backgrounds we used the classical trajectory simulation SAFARI to classify which trajectory types contribute to the background and which contribute to the peaks in the scattered spectra. We found that the background results from trajectories that penetrate through the first layer, and the peaks in the spectra result from QS first layer scattering trajectories. In other words the ions contributing to the peaks have undergone a binary collision with a single surface atom. Figure 7 shows the results of the simulations for 4 keV O and C incident on

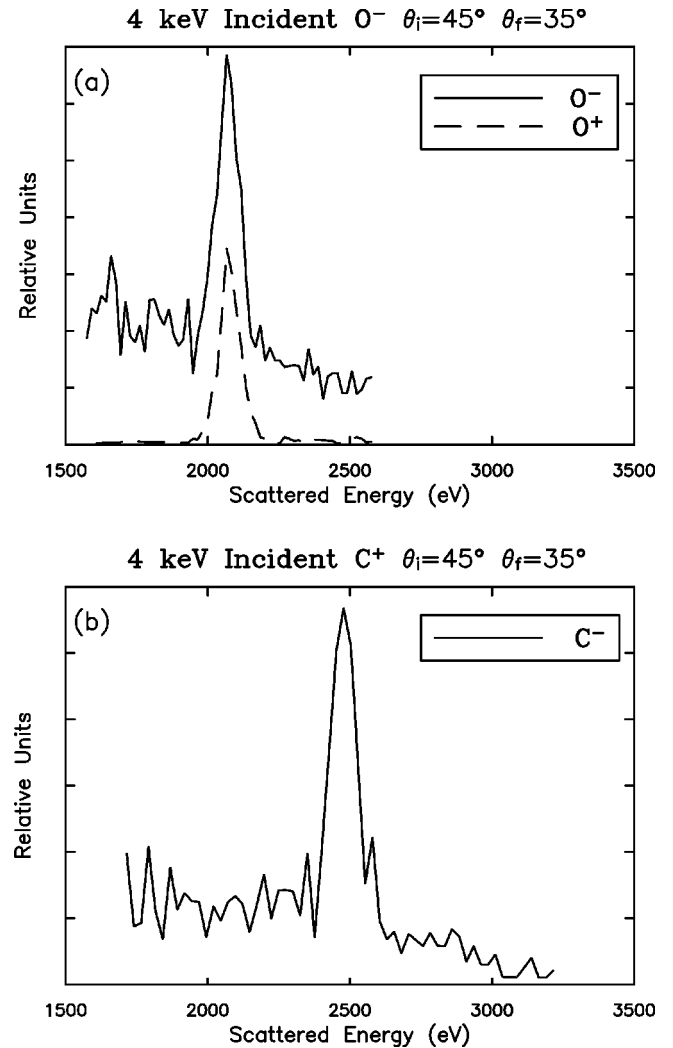


FIG. 6. Comparison of backgrounds in the ESA spectra for ions incident at 4 keV on Cu(001) at  $\theta_i = 45^\circ$ . The final scattering angle is  $\theta_f = 35^\circ$ . (a) Scattered  $O^-$  (solid line) and  $O^+$  (dashed line) spectra. Note that there is almost no background for the  $O^+$  spectrum. (b) Scattered  $C^-$  spectrum. The magnitude of the  $C^-$  background is comparable to that of the scattered  $O^-$  ions. The single scattering peak for C occurs at a higher energy than the O peak, indicating that less energy is lost in the single scattering event for C than O. This reflects the fact that C has a smaller mass than O.

Cu(001) at  $\theta_i = 45^\circ$ . The simulations reproduce the peak positions and the qualitative shapes of the backgrounds for both species. From this we conclude that the charge transfer processes that give rise to the  $C^-$  and  $O^-$  backgrounds are similar, even though the shape of the  $C^-$  angular spectra resemble more closely that of the  $O^+$  angular spectra.

## IV. DISCUSSION

### A. General picture of resonant charge transfer

A discussion of charge transfer that includes many of the key elements needed to understand systems such as O-Cu and C-Cu was given in Ref. 1. Here we reproduce only the details necessary for the present discussion, focusing mainly on nonadiabatic resonant charge transfer. Other relevant processes include Auger charge transfer, which is believed to

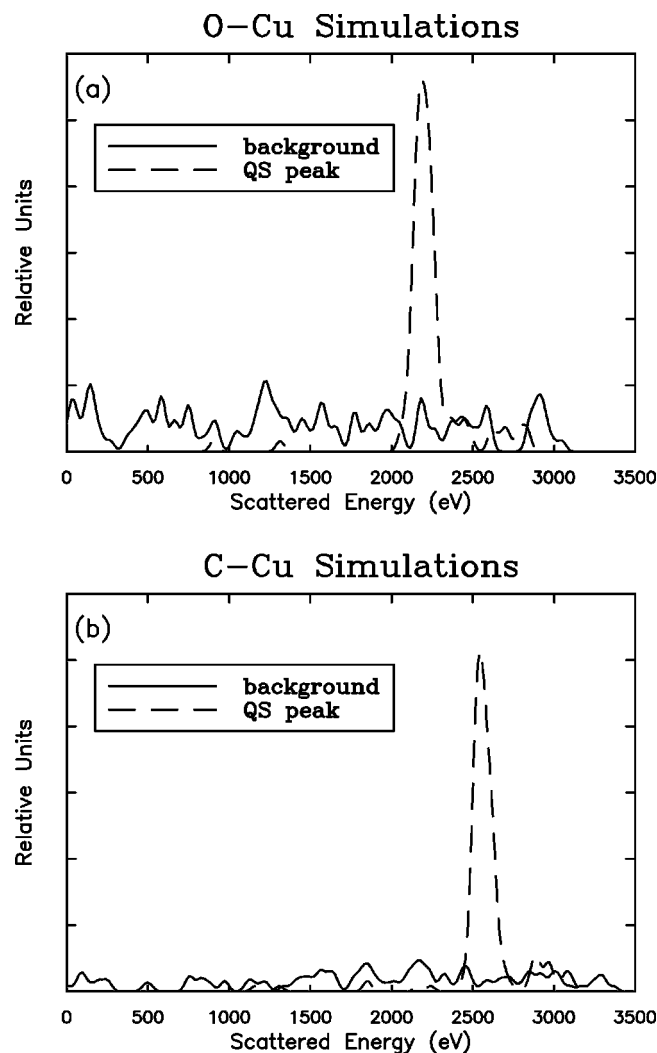


FIG. 7. Calculated energy spectra from the classical trajectory simulation code SAFARI for the scattering of incident (a) O and (b) C from Cu(001) $\langle 100 \rangle$ . The incident ion energy was 4 keV and  $\theta_i = 45^\circ$  and  $\theta_f = 35^\circ$ . Notice that both the scattered O and C spectra are made up of a peak and a background. The peaks result from trajectories that involve QS collisions with surface atoms, and the backgrounds from subsurface scattering trajectories.

play an important role in the neutralization of incident positive ions,<sup>32</sup> a process instrumental in achieving memory loss.

To begin our discussion of resonant charge transfer we must first introduce the basis states we use to describe the O-Cu system. Much of the important physics is determined by the relative energies of these basis states and how they are coupled to one another. Each O-Cu basis state is made up of an atomic oxygen state and a metal state, and there are an infinite number of these O-Cu states due to the continuous nature of the metallic Cu conduction band. The O-Cu states can be divided up into seven subspaces, according to the atomic oxygen states included to describe the system. Figure 8 shows the energies of the lowest energy O-Cu state in each subspace plotted schematically as a function of distance from the surface  $z$ . The lowest energy state of each subspace corresponds to an atomic oxygen state interacting with the lowest energy metal state (i.e., with the metal levels filled up to the Fermi level and no electron-hole pairs). Above each of the states shown in Fig. 8 there is an infinite manifold of

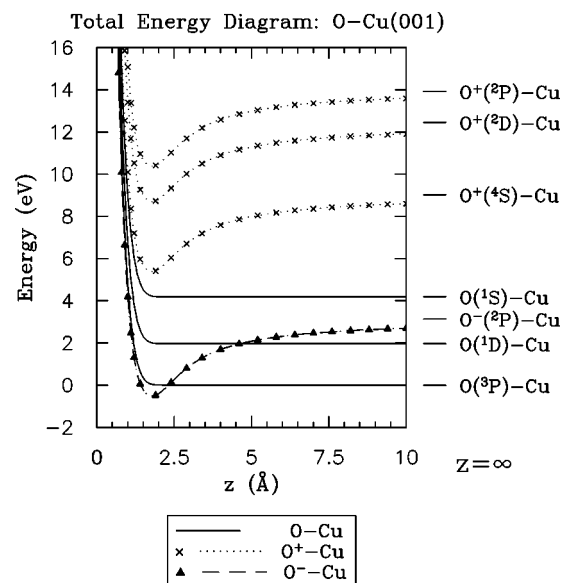


FIG. 8. Energies of selected states for the O-Cu system, drawn schematically for the atomic states interacting with the lowest energy metallic state, i.e., no electron hole pair excitations in the metal. The zero of energy is the  $O(^3P)$ -Cu state at  $z = \infty$ . The energies of the neutral O-Cu system are taken to be constant, and the energies of the  $O^+$ -Cu and  $O^-$ -Cu states decrease with decreasing  $z$  due to the image potential. At very small separations, the energies of all the states increase rapidly due to the strong repulsion of the overlapping oxygen and copper electrons. The clean Cu work function is 4.59 eV. For details on how to obtain the energies of these states see Ref. 13.

states, corresponding to the excited states of the metal (each having a different electron-hole pair distribution), and all of the states have the same  $z$  dependence as the lowest energy state in each subspace. Therefore, we can understand the relative energies of the subspaces by considering the lowest energy state of each subspace alone. For brevity, the lowest energy state of each subspace will now be referred to as an O-Cu state. For more details on this model see Ref. 13.

Since we observe positive ( $2p^3$ ), negative ( $2p^5$ ), and neutral ( $2p^4$ ) oxygen in our experiment and cannot distinguish between ground and excited states, the following atomic oxygen states are considered: the ground state neutral  $O(^3P)$  and two excited states  $O(^1D)$  and  $O(^1S)$ , the negative ion state  $O(^-2P)$ , and the positive ion states  $O^+(^4S)$ ,  $O^+(^2D)$ , and  $O^+(^2P)$ . In Fig. 8, the zero of energy is chosen to be that of the  $O(^3P)$ -Cu state at  $z = \infty$ . The energies of the  $O^+$ -Cu and  $O^-$ -Cu states decrease with decreasing  $z$  due to the image potential, while those of the O-Cu neutral states are taken to be constant. At very small separations the energies of all the O-Cu states increase rapidly due to the repulsion of the overlapping oxygen and copper electrons. Pairs of basis states from different subspaces are coupled to one another by the transfer of an electron between the atom and metal. The couplings between different subspaces are determined from the widths of the relevant ionization and affinity levels,<sup>13</sup> which increase roughly exponentially with decreasing  $z$  until saturation is reached very close to the surface. The larger the coupling, the higher the rate of electron transfer.

The adiabatic ground state wave function of the O-Cu system is a superposition of the basis states. The relative

importance of a given basis state in the adiabatic ground state depends on the relative energies of and couplings between the different O-Cu basis states, and consequently changes continuously with distance. In general, at any given  $z$ , the lowest energy O-Cu states will have the highest probability in the ground state. The probabilities of the basis states in the adiabatic ground state can also be significantly affected<sup>13</sup> when the couplings between states are large (i.e., the system is strongly hybridized). However, for the purpose of this discussion we will focus on the relative energies of the states since these often predict the main contributions to the ground state accurately. We thus expect the relative energies to accurately predict the major final charge state contributions to the scattered flux.<sup>13</sup> It can be seen from Fig. 8 that far from the surface, where the couplings are vanishingly small, the adiabatic ground state is the  $O(^3P)$ -Cu state. Close to the surface the couplings are larger and the adiabatic ground state is an admixture of O-Cu states with the lowest lying  $O(^2P)$ -Cu state having the highest probability.

With these principles in mind, a key element in resonant charge transfer is that, as the ion-surface separation changes during scattering, the system will try to evolve towards the continuously changing ground state by electron transfers between the metal and the atom. Throughout this paper we will assume that the O-Cu system can reach the adiabatic ground state when the atom is close to the surface where the couplings are large and charge transfer is rapid. (The justification for this assumption lies in the observation of memory loss, which we will discuss in more detail in the next section.) However, we will also see that far from the surface the velocity of the scattered atom, together with the exponentially decreasing couplings, will prevent the system from reaching the adiabatic ground state.

### B. Memory loss

In our previous work we measured  $O^+/O^-$  ratios for  $O^+$  incident on Cu(001) in the range of energies from 0.4 to 7 keV, and for a wide range of scattering geometries. One of the primary results was the observation of  $O^+$  ions in the scattered flux, which was unexpected from simple arguments of resonant charge transfer based on the relative energies of the states. At the time it was not possible to experimentally verify that the measured positive ion fractions were not simply due to the survival of the incident  $O^+$ . We have now reproduced these measurements with  $O^-$  incident on Cu(001), over the same range of scattering geometries. Figure 2 compares the results of the two data sets. The data show that within the sensitivity of our measurement, the scattered  $O^+/O^-$  ratio is independent of the incident ion charge state, i.e., memory loss of the incident ion charge state has occurred.

From the observation of memory loss it can be inferred that the state of the O-Cu system close to the surface during, or immediately after, the collision is the same irrespective of the incident ion charge state. We conclude that the charge transfer rate is sufficiently high close to the surface to allow the O-Cu system to equilibrate to the ground state at small separations for both incident  $O^+$  and  $O^-$  ions. Next, we will consider the possible charge transfer mechanisms that can lead to the observation of memory loss.

In the previous section we discussed the idea that in resonant charge transfer the system evolves by attempting to continuously adjust to the changing adiabatic ground state. Within this framework, it is reasonable that resonant charge transfer can lead to memory loss for incident  $O^-$  ions. For incident  $O^+$  ions, however, the situation is significantly different since the system is far from the adiabatic ground state during the incident trajectory. The  $O^+$ -Cu states have very small probabilities in the adiabatic ground state since they lie very high in energy relative to the  $O(^3P)$ -Cu state (see Fig. 8). Thus, we do not expect that resonant charge transfer involving the states of the O-Cu system we have discussed so far will neutralize the incident  $O^+$  ions. Consequently, for the system to equilibrate close to the surface, there must be an alternative explanation for the efficient transfer of electrons to the incident  $O^+$  ions.

The first, and most commonly invoked mechanism, is Auger charge transfer. This is a two-electron process in which one electron neutralizes the incident positive ion, and a second electron is promoted in energy so as to conserve energy. The emission of Auger electrons has been observed by Kempter for 50 eV  $O^+$  ions incident on W(110).<sup>33</sup> A second mechanism involves resonant charge transfer to highly excited neutral O-Cu states that lie close in energy to the  $O^+$ -Cu states. We have not included these states in our discussion so far since they lie much higher in energy than the states shown in Fig. 8, and thus have very small probabilities in the adiabatic ground state of the system. However, on the incident trajectory, when the system is far from equilibrium and resonant charge transfer to the  $O(^3P)$ -Cu,  $O(^1D)$ -Cu, and  $O(^1S)$ -Cu states is highly unlikely, it is possible that there may be resonant charge transfer to the highly excited neutral O-Cu states. These excited neutral O-Cu states can subsequently atomically deexcite to the ground state of the system. This process has been invoked to explain memory loss during the scattering of highly charged O ions.<sup>34</sup>

Our current measurements are not able to distinguish between these two mechanisms and it is possible that both may be occurring simultaneously. However, the quenching of the incident  $O^+$  must be efficient since memory loss of the incident charge state is complete. The efficiency of these processes will be determined, in part, by the rate of electron transfer close to the surface. Unfortunately, the rates for Auger processes are poorly understood and currently unavailable. Similarly the rates for resonant transfer into highly excited neutral states are also unknown. Finally, although memory of the incident  $O^+$  ions is lost, the mechanism for producing scattered  $O^+$  must be able to explain why the outgoing  $O^+$  are not neutralized or converted to  $O^-$  by these same processes.

In summary, since we observe memory loss, we infer that the state of the O-Cu system close to the surface does not depend on the incident ion charge state, and that electronic equilibrium is reached close to the surface. Resonant charge transfer plays an important role in determining memory loss for incident  $O^-$  ions, and there are various possible charge transfer mechanisms responsible for memory loss in the case of the incident  $O^+$  ions. We conclude that, in order to understand the origin of the final measured yields, it is only

necessary to focus on the charge transfer processes occurring during, and after, the collision of the incident ion with the surface.

### C. Nonadiabatic resonant charge transfer

We are now in a position to discuss the effect of the ion's perpendicular velocity on the scattered  $O^-$  and neutral O yields. During ion-surface scattering, the ability of the system to evolve towards the changing ground state is determined by a competition between the ion's perpendicular velocity and the charge transfer rates, which are set by the couplings between the states (or, equivalently, by the widths of the relevant ionization and affinity levels). With this in mind, it is necessary to consider what effect the ion velocity has on the final measured yields. Close to the surface the O-Cu system is in the ground state, where the  $O^-(^2P)$ -Cu state is the most energetically favored. As the ion leaves the surface, it becomes more energetically favorable for the system to be in the  $O(^3P)$ -Cu state. For small perpendicular velocities, it is possible for electron transfers to track this changing ground state (up to some value of  $z$  at which the widths become very small). However, the faster a negative ion leaves the surface, i.e., the higher its final perpendicular velocity, the harder it is for electron transfers to enable the system to track the adiabatic ground state. This corresponds to a higher negative ion yield at higher incident ion energies (for a given scattering geometry) since the scattered ions have higher perpendicular velocities. This is consistent with the TOF data presented in Fig. 4, where the negative ion yields gradually increase with increasing incident ion energy, for both scattering geometries. It is also consistent with the fact that the negative ion yield is greater for  $\theta_f=45^\circ$ , which corresponds to a perpendicular velocity of  $0.942 \times 10^{-3} \sqrt{E_i}$  (a.u.), than for  $\theta_f=65^\circ$ , which corresponds to a perpendicular velocity of  $0.853 \times 10^{-3} \sqrt{E_i}$  (a.u.).

Finally, using this simple model of resonant charge transfer we can conclude that, since the  $O^+$ -Cu states lie relatively high in energy, it is rather surprising to see any  $O^+$  ions in the scattered flux. In the next section we will propose an alternative mechanism for the production of  $O^+$  ions, which relies on the hardness of the collision between the incident oxygen ions and the surface Cu atoms.

### D. Evidence that $O^+$ production is due to a collisional mechanism

Above we presented a simple model that qualitatively explained the behavior of the observed  $O^-$  and neutral O yields, but cannot explain the presence, or behavior, described in detail below, of the  $O^+$  yields. These yields can also not be explained in terms of the parallel velocity mechanism introduced in Ref. 35. Our  $O^+$  yields decrease with increasing parallel velocity, contrary to the predictions made in Ref. 35. Instead, we show here that our data support the hypothesis that a collisional mechanism, originally suggested by Maazouz *et al.*<sup>8</sup> for similar systems (O-Mg, O-Al, and O-Ag), is responsible for the  $O^+$  yields.

During a hard collision between the incident projectile and a surface Cu atom, the atomic levels of the target and projectile merge into molecular orbitals (MOs). As the atoms

separate, electrons can be trapped in excited atomic levels at MO crossings.<sup>36</sup> Thus, the final charge state of an ion or atom can be influenced by excitations that result from electron promotions within molecular orbitals (MO's). For a given scattering geometry, these excitations are most pronounced at high incident energies, where the distance of closest approach is smallest.

Maazouz *et al.*<sup>8</sup> have suggested that these collisional excitations may result in the production of highly excited neutral oxygen atoms  $O^{**}$ .<sup>37</sup> These highly excited atoms can survive the outgoing trajectory and then deexcite by an atomic Auger process in which an electron is emitted, a process called autoionization. Due to the long lifetimes of the excited states,<sup>36</sup> these autoionization processes occur far from the surface where the resulting  $O^+$  ions are unlikely to suffer additional neutralization. Autoionizing states result in both the presence of positive ions in the scattered flux and in emission of electrons with energies characteristic of the autoionizing state. Electron promotion within molecular orbitals has been invoked previously<sup>24-27</sup> to explain high positive ion yields. Maazouz *et al.*<sup>8</sup> have suggested that the lowest energy autoionizing state of O is the  $O^{**}$  ( $2p^23s^2$ ), with an energy of 17.75 eV above the neutral ground state.

Another possible mechanism that can explain the observation of scattered  $O^+$ , still within the framework of electron promotion during the hard collision, involves the promotion of a single O  $2p$  electron. As the O and Cu separate this electron may become trapped in the Cu  $4s$  orbital, resulting in the direct production of  $O^+$  ions at very small ion-surface separations. However, if this process is responsible for the observation of  $O^+$  ions, it is difficult to explain why incident  $O^+$  ions are efficiently neutralized on the incident trajectory, which we infer from our observation of memory loss, while the  $O^+$  ions created directly in the hard collision can survive the outgoing trajectory. As will be seen below, it is possible to conclude from our data that a hard collision is involved in the creation of positive ions, but it is not possible to determine the exact mechanism.

The data shown in Fig. 4(b) provide supporting evidence that the positive ion fractions are produced by a collisional mechanism. The positive ion yield  $P^+$  turns on above some incident ion energy and is zero below this energy, within the sensitivity of our measurement. This result suggests that there is a minimum collisional energy required to "turn-on" positive ion production. It can also be seen from Fig. 4(b) that  $P^+$  is smaller for the more grazing scattering geometry at a fixed incident energy, which is consistent with this type of mechanism since a more grazing scattering geometry also corresponds to a less violent collision. Finally, the data shown in Fig. 4(b) are very similar to those shown in Ref. 27, in which there is a sharp increase at 4 keV incident ion energy in the scattered  $Ne^+$  yields, which were also explained via a collisional mechanism.

Further evidence for a collisional mechanism is seen in Fig. 6(a), which compares the scattered  $O^+$  and  $O^-$  spectra for  $O^-$  incident on Cu(001) with  $\theta_i=45^\circ$  and  $\theta_f=35^\circ$ . It can be seen that the magnitude of the background in the scattered  $O^+$  spectrum is significantly smaller than that for the scattered  $O^-$  spectrum. Furthermore, the results of the classical trajectory simulation (see Fig. 7 and Sec. III D) show that the peaks result from QS type trajectories, in

which the incident ion has undergone a collision predominantly with a single surface atom, while the backgrounds result from subsurface trajectories. Since we do not see a background in the  $O^+$  spectra, either the scattered  $O^+$  ions are created only in QS surface collisions or, if they are created subsurface, they do not survive the outgoing trajectory.

One method to determine the importance of the collision in producing positive ions is to measure electron spectra, looking for evidence of the proposed autoionizing states. These states are revealed as electrons emitted at the energy corresponding to the autoionizing decay process. Such electrons have been observed for Ne and other noble gas scattering experiments. For example, a peak in the electron spectra has been observed at the correct energy for the decay of the  $Ne^{**}$  ( $2p^4 3s^2$ ) autoionizing states.<sup>28,29</sup> Similarly, electrons due to  $O^{**}$  autoionizing states have been observed in gas-phase collisions.<sup>38</sup> However, electron spectra for  $O^+$  scattering from Mg revealed no peak due to the  $O^{**}$  autoionizing state.<sup>8</sup> One should note that in Ref. 8, the authors did not expect to see any such peaks since the incident ion beam current was too low for a significant number of the autoionizing states to be created, leading to an electron count rate (from the autoionizing states) that was too low to be measurable. Therefore, more conclusive measurements are needed to determine directly if the hard binary collision with a single surface atom results in autoionizing states responsible for the observed  $O^+$  ion fractions.

In conclusion, our results point to a mechanism of  $O^+$  production that depends on the strength of the hard collision between the incident ion and surface atom. However, it should be noted that the difference between the positive ion yields at  $\theta_f = 45^\circ$  and  $\theta_f = 65^\circ$ , shown in Fig. 4(b), is also consistent with the  $O^+$  ions spending more time in the near-surface region at  $\theta_f = 65^\circ$ , which could result in higher neutralization probabilities for any  $O^+$  ions that are produced. Therefore, the smaller yields at larger  $\theta_f$  are a result of both lower production rates and higher neutralization.

### E. The C-Cu(001) system

In the previous sections we saw that the measured  $O^-$  and neutral O atom yields can be explained by nonadiabatic resonant charge transfer and that a collisional mechanism can explain the measured  $O^+$  ion yields. Here we will see that the scattered  $C^-$  fractions are also consistent with a simple resonant charge transfer model, while no  $C^+$  ions were observed for any incident ion energy or scattering geometry. C is an interesting complementary system to study since neutral C has two  $p$  electrons in the outer valence band, whereas neutral O has two holes in the outer valence band. As a result, a basic description of the C-Cu system includes many states with orbital symmetries similar to those of the O-Cu system: the ground state neutral ( $2p^2$ )  $C(^3P)$  and two excited states  $C(^1D)$  and  $C(^1S)$ , the positive ion state ( $2p^1$ )  $C^+(^2P)$ , and the negative ion states ( $2p^3$ )  $C^-(^4S)$ , and  $C^-(^2D)$ . The  $C^-(^2P)$  is not included since it is not bound and, in fact, the  $C^-(^2D)$  is only weakly bound by 35 meV. Figure 9 shows the energies of the C-Cu states as a function of distance from the surface.

It can be seen from Fig. 9 that the  $C(^3P)$ -Cu state is always the most energetically favorable and will contribute

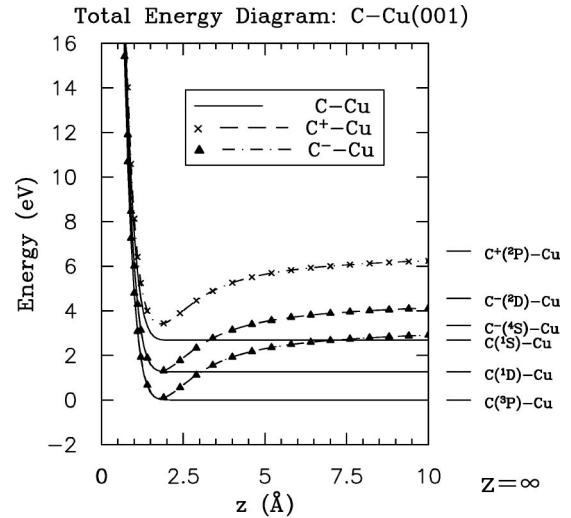


FIG. 9. Energies of selected states for the C-Cu system, drawn schematically for the atomic states interacting with the lowest energy metallic level. The zero of energy is the  $C(^3P)$ -Cu state at  $z = \infty$ . The energies of the neutral C-Cu system are taken to be constant, and the energies of the  $C^+$ -Cu and  $C^-$ -Cu states decrease with decreasing  $z$  due to the image potential. At very small separations, the energies of all the states increase rapidly due to the strong repulsion of the overlapping carbon and copper electrons.

significantly to the adiabatic ground state wave function of the C-Cu system. This is in contrast to the O-Cu system where, close to the surface, the  $O^-(^2P)$ -Cu state is the most energetically favorable state. Due to the hybridization of states close to the surface the  $C^-(^4S)$ -Cu state will also contribute significantly to the C-Cu ground state wave function. Consequently, there is a finite probability of  $C^-$  ions surviving the outgoing trajectory, resulting in our observation of  $C^-$  ions in the scattered flux. Absolute yields for the C-Cu system are not available at this time; however, we expect the  $C^-$  yields to be smaller than the  $O^-$  yields since the  $C^-(^4S)$ -Cu state is higher in energy than the  $O^-(^2P)$ -Cu state, relative to the respective lowest energy states of the two systems.

To illustrate that our scattered  $C^-$  data are consistent with a model of resonant charge transfer we examine the similarity between the magnitudes of the backgrounds in the scattered  $O^-$  and  $C^-$  spectra which contrast sharply with the much smaller magnitude of the  $O^+$  background (see Fig. 6). This similarity suggests that the general charge transfer mechanisms determining the  $O^-$  and  $C^-$  yields are similar in origin, i.e., both are determined by resonant charge transfer. We can also conclude from a comparison of the  $C^-$  and  $O^-$  angular spectra that the  $C^-$  yields are more sensitive to the perpendicular velocities of the scattered ions than the  $O^-$  yields (see Fig. 5). As we noted in Sec. III D, the envelope connecting the QS peaks in the  $C^-$  angular spectrum of Fig. 5(c) does not have the shape expected from the scattering cross section alone. Specifically, the  $C^-$  intensity is largest at the most normal scattering geometries, where the outgoing perpendicular velocity is largest, indicating that the shape is dominated by charge transfer processes. In contrast, the  $O^-$  angular spectrum in Fig. 5(a) is more typical of one dominated by the scattering cross section, in which the intensity is largest at  $\theta_f = 65^\circ$ . Thus we conclude that the scattered  $C^-$

yields are more sensitive to the perpendicular velocity of the scattered ions than the  $O^-$  yields.

Finally, in the previous sections we have shown that resonant charge transfer cannot explain our measured  $O^+$  ion yields since the  $O^+$ -Cu states lie very high in energy and are never expected to have significant probabilities in the adiabatic ground state. Similarly, since the  $C^+$ -Cu state lies very high in energy, we do not expect to observe any  $C^+$  ions in the scattered flux due to nonadiabatic resonant charge transfer alone. In fact, further evidence that  $O^+$  production is due to a charge transfer mechanism different from resonant charge transfer lies in the fact that the  $O^+$ -Cu states lie higher in energy than the  $C^+$ -Cu states (relative to the O-Cu and C-Cu ground states, respectively.) Consequently, if positive ion production in the C-Cu and O-Cu systems was due to resonant charge transfer, one would expect to observe more scattered  $C^+$  than  $O^+$ . However, no scattered  $C^+$  ions were observed at any incident ion energy or scattering geometry under investigation, and this is consistent with our simple picture of nonadiabatic resonant charge transfer and with the hypothesis that the  $O^+$  ions are created during the hard collision with the surface atoms.

## V. CONCLUSION

We have measured the absolute yields of  $O^+$ ,  $O^-$ , and neutral oxygen resulting from the scattering of low-energy  $O^+$  and  $O^-$  from Cu(001). This provides a comprehensive data set that can be compared to the results of models that correctly incorporate the effects of multiple  $p$  electrons in a

dynamical multistate system. Accurate measurements of the  $O^+/O^-$  ratios for both incident charge species show that memory loss of the incident charge state is complete over a broad range of scattering energies and geometries. From this we conclude that the incident  $O^+$  ions are efficiently neutralized by an Auger process or by a combination of Auger processes and resonant charge transfer into excited neutral states. We have found that the scattered  $O^+$  ions are produced by a collision mechanism during the hard collision with the surface Cu atoms, and  $O^-$  ions are present in the scattered flux due to nonadiabatic resonant charge transfer. We have also investigated the scattering of low energy  $C^+$  from Cu(001). The  $C^-$  angular spectra have been compared to  $O^+$  and  $O^-$  angular spectra, demonstrating that the observed  $C^-$  ions are also due to resonant charge transfer. No measurable yield of  $C^+$  ions is observed in the scattered flux.

## ACKNOWLEDGMENTS

We wish to thank J.P. Gauyacq and E.B. Dahl for useful discussions concerning the interpretation of the data. We would also like to thank R.A. Baragiola for his assistance in constructing and interpreting the one-electron MO orbital correlation diagrams. This research was supported by the National Science Foundation (Grant Nos. NSF-DMR-9313818 and NSF-DMR-9722771). Additional support was provided by the Air Force Office of Scientific Research (Grant No. AFOSR-91-0137). C.A.K. received primary support from the Fannie and John Hertz Foundation.

\*Recently deceased.

<sup>1</sup>C. A. Keller, A. C. Lavery, and B. H. Cooper, *Phys. Rev. B* **58**, 10 959 (1998).

<sup>2</sup>D. Teillet-Billy, B. Bahrim, and J. P. Gauyacq, *Nucl. Instrum. Methods Phys. Res. B* **100**, 296 (1995).

<sup>3</sup>B. Bahrim, D. Teillet-Billy, and J. P. Gauyacq, *Phys. Rev. B* **50**, 7860 (1994).

<sup>4</sup>S. Ustaze, L. Guillemot, V. A. Esaulov, P. Nordlander, and D. C. Langreth, *Surf. Sci.* **415**, L1027 (1998).

<sup>5</sup>B. Bahrim, A. G. Borisov, D. Teillet-Billy, J.-P. Gauyacq, F. Wieggershaus, St. Krischok, and V. Kempter, *Surf. Sci.* **380**, 556 (1997).

<sup>6</sup>D. Teillet-Billy and J. P. Gauyacq, *Surf. Sci.* **239**, 343 (1990).

<sup>7</sup>M. Maazouz, S. Ustaze, L. Guillemot, and V. A. Esaulov, *Surf. Sci.* **409**, 189 (1998).

<sup>8</sup>M. Maazouz, L. Guillemot, T. Schlatholter, S. Ustaze, and V. A. Esaulov, *Nucl. Instrum. Methods Phys. Res. B* **125**, 283 (1997).

<sup>9</sup>H. M. van Pinxteren, C. F. A. van Os, R. M. A. Heeren, R. Rodink, J. J. C. Geerlings, and J. Los, *Europhys. Lett.* **10**, 715 (1989).

<sup>10</sup>B. Hird, P. Gauthier, J. Bulicz, and R. A. Armstrong, *Phys. Rev. Lett.* **67**, 3575 (1991).

<sup>11</sup>J. B. Marston, D. R. Andersson, E. R. Behringer, B. H. Cooper, C. A. DiRubio, G. A. Kimmel, and C. Richardson, *Phys. Rev. B* **48**, 7809 (1993).

<sup>12</sup>Hongxiao Shao, D. C. Langreth, and P. Nordlander, *Phys. Rev. B* **49**, 13 929 (1994).

<sup>13</sup>E. B. Dahl, E. R. Behringer, D. R. Andersson, and B. H. Cooper,

*Int. J. Mass Spectrom. Ion Phys.* **174**, 267 (1998); E. B. Dahl, Ph.D. thesis, Cornell University, 1998.

<sup>14</sup>E. R. Behringer, D. R. Andersson, B. H. Cooper, and J. B. Marston, *Phys. Rev. B* **54**, 14 765 (1996); **54**, 14 780 (1996).

<sup>15</sup>G. A. Kimmel and B. H. Cooper, *Rev. Sci. Instrum.* **64**, 672 (1993).

<sup>16</sup>R. L. McEachern, D. L. Adler, D. M. Goodstein, G. A. Kimmel, B. R. Litt, D. R. Peale, and B. H. Cooper, *Rev. Sci. Instrum.* **59**, 2560 (1988).

<sup>17</sup>D. L. Adler and B. H. Cooper, *Rev. Sci. Instrum.* **59**, 137 (1988).

<sup>18</sup>M. Menzinger and L. Wählin, *Rev. Sci. Instrum.* **40**, 102 (1969).

<sup>19</sup>Galileo Electron-Optics Corp. Channeltron model 4830.

<sup>20</sup>C. A. Keller and B. H. Cooper, *Rev. Sci. Instrum.* **67**, 2760 (1996).

<sup>21</sup>D. M. Goodstein, S. A. Langer, and B. H. Cooper, *J. Vac. Sci. Technol. A* **6**, 703 (1988).

<sup>22</sup>P. Biersack and J. F. Ziegler, in *Ion Implantation Techniques*, Springer Series in Electrophysics Vol. 10, edited by H. Ryssel and H. Glawischnig (Springer-Verlag, Berlin, 1982).

<sup>23</sup>The ZBL potential is a universal potential that depends only on the atomic numbers of the projectile and target atoms. It has been successfully used to reproduce the scattering of 500–2500 eV  $Li^+$ ,  $Na^+$ , and  $K^+$ , from Mo(001) (Ref. 22). Our classical trajectory simulation does not include charge transfer and, consequently, can only be used to perform trajectory analysis and not to predict final charge state yields.

<sup>24</sup>F. Xu, G. Manico, F. Ascione, A. Bonanno, A. Oliva, and R. A.

- Baragiola, Phys. Rev. A **57**, 1096 (1998).
- <sup>25</sup>O. Grizzi, M. Shi, H. Bu, J. W. Rabalais, and R. A. Baragiola, Phys. Rev. B **41**, 4789 (1990).
- <sup>26</sup>J. W. Rabalais, Jie-Nan Chen, R. Kumar, and M. Narayana, J. Chem. Phys. **83**, 6489 (1985).
- <sup>27</sup>T. M. Buck, W. E. Wallace, R. A. Baragiola, G. H. Wheatley, J. B. Rothman, R. J. Gorte, and J. G. Tittensor, Phys. Rev. B **48**, 774 (1993).
- <sup>28</sup>G. Zampieri, F. Meier, and R. Baragiola, Phys. Rev. A **29**, 116 (1984).
- <sup>29</sup>V. A. Esaulov, S. Lacombe, L. Guillemot, and Vu Ngoc Tuan, Nucl. Instrum. Methods Phys. Res. B **100**, 232 (1995).
- <sup>30</sup>B. H. Wolf, in *Handbook of Ion Sources*, edited by B. H. Wolf (CRC Press, Boca Raton, 1995).
- <sup>31</sup>D. L. Adler and B. H. Cooper, Phys. Rev. B **43**, 3876 (1991).
- <sup>32</sup>K. J. Snowdon, R. Hentschke, A. Narmann, W. Heiland, E. Mühling, and W. Eckstein, Nucl. Instrum. Methods Phys. Res. B **23**, 309 (1987).
- <sup>33</sup>H. Müller, G. Gador, H. Brenten, and V. Kempter, Surf. Sci. **313**, 188 (1994).
- <sup>34</sup>A. Arnau, F. Aumayr, P. M. Echenique, M. Grether, W. Heiland, J. Limburg, R. Morgenstern, P. Roncin, S. Schippers, R. Schuch, N. Stolterfoht, P. Varga, T. J. M. Zouros, and H. P. Winter, Surf. Sci. **27**, 113 (1997).
- <sup>35</sup>C. Auth, H. Winter, A. G. Borisov, B. Bahrim, D. Teillet-Billy, and J. P. Gauyacq, Phys. Rev. B **57**, 12 579 (1998).
- <sup>36</sup>M. Barat and W. Lichten, Phys. Rev. A **6**, 211 (1972).
- <sup>37</sup>We have constructed the one-electron diabatic MO correlation diagram for the O-Cu system, following the Barat-Lichten rules (Ref. 36). We have seen that the O( $2p$ ) orbital is strongly promoted, correlated with the  $4f\sigma$  MO, and crosses empty MO's of the same symmetry. We infer from this that the electron promotions proposed here to explain O<sup>+</sup> and O<sup>\*\*</sup> production may occur, although further work is necessary to determine the relative probabilities of these promotions. There are further complications in interpreting these diagrams since the Cu conduction band electrons lie close in energy to both the Cu( $3d$ ) and Cu( $4s$ ) orbitals and are also resonant with the relevant O-Cu MO crossings.
- <sup>38</sup>F. Penent, J. P. Grouard, R. I. Hall, J. L. Montmagnon, R. L. Champion, L. D. Doverspike, and V. A. Esaulov, J. Phys. B **20**, 6065 (1987).